Hierarchical Algorithms for Causality Retrieval in Atrial Fibrillation Intracavitary Electrograms

David Luengo, *Member, IEEE,* Gonzalo Ríos-Muñoz, Víctor Elvira, *Member, IEEE,* Carlos Sánchez, Antonio Artés-Rodríguez, *Senior Member, IEEE,*

***Abstract*—Multi-channel intracavitary electrograms (EGMs), are acquired at the electrophysiology laboratory to guide radio frequency catheter ablation of patients suffering from atrial fibrillation (AF). These EGMs are used by cardiologists to determine candidate areas for ablation (e.g., areas corresponding to high dominant frequencies or complex fractionated electrograms). In this paper, we introduce two hierarchical algorithms to retrieve the causal interactions among these multiple EGMs. Both algorithms are based on Granger causality, but other causality measures can be easily incorporated. In both cases, they start by selecting a root node, but they differ on the way in which they explore the set of signals to determine their cause-effect relationships: either testing the full set of unexplored signals (GS-CaRe) or performing a local search only among the set of neighbor EGMs (LS-CaRe). The ensuing causal model provides important information about the propagation of the electrical signals inside the atria, uncovering wavefronts and activation patterns that can guide cardiologists towards candidate areas for catheter ablation. Numerical experiments, on both synthetic signals and annotated real-world signals, show the good performance of the two proposed approaches.**

***Index Terms*—electrocardiography, intracavitary electrograms, atrial fibrillation, radio frequency ablation, Granger causality**

1. Introduction

ATRIAL fibrillation (AF) is a cardiac pathology characterized by a rapid and unsynchronized contraction of the atria. AF is the most common cardiac arrhythmia in clinical practice [1], having reached epidemic proportions: one out of four people over 40 years old are predicted to suffer from AF throughout their lifetime [2]. Although AF is not deadly *per se*, it causes a substantial discomfort on patients, results in a large number of hospitalizations and is an important risk factor for other pathologies like sudden death [3] or stroke [4]. However, the underlying causes for the initiation and maintenance of AF are still not fully understood, and several hypotheses have been proposed [5], [6]. The prevailing hypothesis for AF maintenance still relies on the existence of multiple wavelets randomly propagating through the atria [7], [8]. More recently it has been hypothesized that stable spatio-temporal re-entrant waves (rotors) may be responsible for AF initiation and maintenance [9]. According to this theory, ablating those specific areas of the myocardium should lead to AF termination. Consequently, radio frequency (RF) ablation, where an RF catheter is introduced inside the heart and used to ablate potentially arrhythmogenetic areas, is increasingly used. This approach has shown promising results for paroxysmal AF patients, with success rates around 70–80 % by performing pulmonary vein isolation (PVI), but has not been so effective for persistent AF [10]. In this case, other ablation strategies (e.g., ablating areas with complex fractionated EGMs [11] or high dominant frequencies [12]) have been tested, but their results are still unsatisfactory in many cases.[1]

The lack of satisfactory performance of RF ablation strategies for some patients is our main motivation. We believe that there is an urgent need of more advanced signal processing and machine learning methods that can assist cardiologists during RF ablation therapies. These techniques should focus on determining the direction of information transfer in the multiple EGMs recorded in the electrophysiology laboratory. This information will help both to better understand the propagation of the action potential (AP) inside the atria of AF patients and to identify candidate sites for RF ablation. With these goals in mind, Granger causality (G-causality or GC) is a well established methodology to infer causal relations among multiple time series [15]. Several authors have investigated the inference of causality relationships among different biomedical signals [16], [17]. In particular, causality discovery tools have been extensively used in neurology [15], and GC has been used to investigate the relationship between several physiological time series (heart period, arterial pressure and respiration variability) [18], [19]. The use of partial directed coherence to investigate propagation patterns in intra-cardiac signals was considered in [20], [21], whereas GC maps have been built in [22], [23], [24]. However, all of these approaches are based on the standard approach to causality discovery, i.e., computing the pairwise or full-conditional G-causality as described in Section 2. More recently, [25] proposed alternative multivariate causality measures that involve the computation of GC conditioned only on neighbor nodes.

In this paper, a hierarchical framework for causality retrieval in EGMs is described. The first stage of the proposed method-

D. Luengo is with the Department of Signal Theory and Communications, Universidad Politécnica de Madrid, 28031 Madrid (Spain). E-mail: david.luengo@upm.es

G. Ríos-Muñoz and A. Artés-Rodríguez are with the Department of Signal Theory and Communications (Universidad Carlos III de Madrid) and Gregorio Marañón Health Research Institute, Madrid (Spain). E-mails:{griosm,antonio}@tsc.uc3m.es

V. Elvira is with IMT Lille Douai, Université de Lille, and CRIStAL laboratory (UMR 9189), France. E-mail: victor.elvira@imt-lille-douai.fr

C. Sánchez is with the Defense University Centre (CUD) of the General Military Academy of Zaragoza (AGM), the Biosignal Interpretation and Computational Simulation (BSICoS) Group (Universidad de Zaragoza), and Centro de Investigacin Biomédica en Red (CIBER-BBN).

[1]Complex fractionated EGMs are electrograms that do not exhibit the quasi-periodic shape of regular electrograms, but a much more complex and irregular shape [13]. The dominant frequency (DF) corresponds to the highest peak of the frequency spectrum measured in a certain area inside the atria [14].

ology consists of finding the EGM having the "strongest" GC links with other EGMs and selecting it as the root node. The remaining nodes are then processed sequentially, starting from the set of candidate children of the root node. Two alternative algorithms are proposed for this purpose: global search causal retrieval (GS-CaRe) and local search causal retrieval (LS-CaRe). GS-CaRe processes the candidate children of the current node sequentially according to their causal strength, accepting them as true children if their GC is statistically significant conditioned on all the previously accepted children. LS-CaRe also processes the candidate children sequentially, but only takes into account the neighbor nodes, thus avoiding many false alarms. An exhaustive evaluation of the proposed algorithms has been performed, using both synthetic signals and annotated real-world signals from AF patients acquired at the electrophysiology laboratory of Hospital General Universitario Gregorio Marañón (HGUGM). Note that the GS-CaRe algorithm was already described in [26], [27]. With respect to [26], [27], a completely novel algorithm (LS-CaRe) is proposed, and an exhaustive set of simulations (using synthetic and real data) are performed to validate both algorithms.

The rest of the paper is organized as follows. Firstly, Section 2 provides an introduction to Granger causality, describing both pairwise and conditional causality. The notation used throughout the text is also summarized here in Table I. Then, Section 3 describes the two hierarchical causality discovery algorithms proposed: GS-CaRe and LS-CaRe. This is followed by Section 4, where numerical experiments (using both synthetic and real data) are used to validate the developed algorithms. Finally, the paper is closed in Section 5 with a discussion that includes potential future lines.

2. Granger Causality

A. Pairwise Causality

Let us assume that we have N samples of a multi-variate time series composed of Q interrelated signals, $x_q[n]$ for $q = 1, \ldots, Q$ and $n = 0, 1, \ldots, N-1$. Granger causality measures the increase in predictability on the future outcome of a signal, $x_q[n]$, given the past values of another signal, $x_\ell[n]$ with $\ell \neq q$, with respect to (w.r.t.) the predictability achieved by taking into account only past values of $x_q[n]$ [15], [28]. In short, G-causality determines whether past values of $x_\ell[n]$ can be useful to forecast future values of $x_q[n]$ or not.

In order to provide a rigorous formulation of GC, let us define the linear autoregressive (AR) predictor for $x_q[n]$ given its past samples (i.e., the q-th *self-predictor*) as

$$\hat{x}_q[n] = \hat{x}_{q\to q}[n] = \sum_{m=1}^{M} \alpha_{qq}[m] x_q[n-m] = \boldsymbol{\alpha}_{qq}^\top \mathbf{x}_q[n], \quad (1)$$

where M is the order of the predictor, obtained typically using some penalization for model complexity to avoid overfitting [29]; $\alpha_{qq}[m]$ are the coefficients of the model; $\boldsymbol{\alpha}_{qq} = [\alpha_{qq}[1], \ldots, \alpha_{qq}[M]]^\top$ and $\boldsymbol{\alpha}_{qq}^\top$ denotes the transpose of $\boldsymbol{\alpha}_{qq}$; and $\mathbf{x}_q[n] = [x_q[n-1], \ldots, x_q[n-M]]^\top$. Similarly, let us define the linear AR predictor for $x_q[n]$ given the past samples of both $x_q[n]$ and $x_\ell[n]$ (i.e., the *cross-predictor* from the ℓ-th signal to the q-th signal) as

$$\hat{x}_{\ell\to q}[n] = \boldsymbol{\alpha}_{qq}^\top \mathbf{x}_q[n] + \boldsymbol{\alpha}_{\ell q}^\top \mathbf{x}_\ell[n] = \hat{x}_q[n] + \boldsymbol{\alpha}_{\ell q}^\top \mathbf{x}_\ell[n], \quad (2)$$

where $\boldsymbol{\alpha}_{\ell q} = [\alpha_{\ell q}[1], \ldots, \alpha_{\ell q}[M]]^\top$; $\mathbf{x}_\ell[n] = [x_\ell[n-1], \ldots, x_\ell[n-M]]^\top$; and $\hat{x}_q[n]$ is given by (1).

The *residual errors* of these two predictors in (1) and (2) can now be defined as $\varepsilon_q[n] = x_q[n] - \hat{x}_q[n]$ and $\varepsilon_{\ell\to q}[n] = x_q[n] - \hat{x}_{\ell\to q}[n]$, respectively. The *pairwise G-causality* strength is then measured by the logarithm of the ratio of the two variances of the residuals [30]:

$$G_{\ell\to q} = \ln \frac{\mathrm{Var}(\varepsilon_q[n])}{\mathrm{Var}(\varepsilon_{\ell\to q}[n])}. \quad (3)$$

Note that $\mathrm{Var}(\varepsilon_{\ell\to q}[n]) \approx \mathrm{Var}(\varepsilon_q[n])$ when $\mathbf{x}_\ell[n]$ does not provide any useful information w.r.t. $x_q[n]$, whereas $\mathrm{Var}(\varepsilon_{\ell\to q}[n]) < \mathrm{Var}(\varepsilon_q[n])$ if $\mathbf{x}_\ell[n]$ allows us to improve the prediction of $x_q[n]$. Hence, $0 \leq G_{\ell\to q} < \infty$, with larger values of $G_{\ell\to q}$ indicating a stronger evidence of causality from ℓ to q. Using these pairwise values, we can build a *pairwise G-causality strength matrix*, $\mathbf{G}$, such that its (ℓ, q)-th entry is given by[2]

$$\mathbf{G}_{\ell,q} = \begin{cases} G_{\ell\to q}, & \ell \neq q; \\ 0, & \ell = q. \end{cases} \quad (4)$$

Finally, it is important to remark that we should add a causality link from ℓ to q only when the decrease in the residual's noise variance from (1) to (2) is statistically significant. In order to construct this causality graph, we define the *pairwise G-causality connection matrix*, $\mathbf{C}$, whose (ℓ, q)-th element is

$$\mathbf{C}_{\ell,q} = \begin{cases} 1, & \chi(G_{\ell\to q}) \leq \gamma; \\ 0, & \chi(G_{\ell\to q}) > \gamma, \end{cases} \quad (5)$$

where $\chi(G_{\ell\to q})$ denotes some appropriate statistic and γ is the threshold value (i.e., significance level) used to determine whether the value of $G_{\ell\to q}$ is statistically significant. In order to retrieve the potential causality link between two nodes, we resort to p-values, and thus we denote $\gamma = \gamma_p$ [31].[3] The typical values of p in biomedical engineering which will be used here are $p = 0.05$, $p = 0.01$ or $p = 0.001$. Finally, for the sake of simplicity we will use the following short-hand notation for $\mathbf{C}_{\ell,q}$ in (5):

$$\mathbf{C}_{\ell,q} = [\![\chi(G_{\ell\to q}) \leq \gamma_p]\!], \quad (6)$$

where $[\![\mathcal{LC}]\!] = 1$ if the logical condition $\mathcal{LC}$ is true and $[\![\mathcal{LC}]\!] = 0$ otherwise (i.e., if $\mathcal{LC}$ is false), whereas γ_p is the threshold value obtained from the corresponding user-defined p-value.

[2]Note that $\mathrm{Var}(\varepsilon_{q\to q}[n]) = \mathrm{Var}(\varepsilon_q[n])$, since $\hat{x}_q[n] = \hat{x}_{q\to q}[n]$, and thus the definition in (4) is consistent with (3), since $G_{q\to q}[n] = \ln 1 = 0$.

[3]Let us note that some alternative and more complicated approaches than p-values have been proposed in the literature [32]. However, p-values are simple to understand and set by the users, their use is widespread in biomedical applications (as well as in other scientific areas), and they are enough for our purposes. Indeed, we have tested several values of p in the simulations (see Section 4), noticing that the value of p has little influence on the results, as long as it is small enough (i.e., $p \leq 0.05$).

TABLE I
SUMMARY OF THE MAIN NOTATION USED IN THE DEFINITION OF THE HIERARCHICAL GRANGER CAUSALITY ALGORITHM.

Variable	Description
$x_q[n]$	Observed signals ($1 \leq q \leq Q$, $0 \leq n \leq N-1$).
$M_{\ell q}$	Maximum delay in the prediction from the ℓ-th to the q-th signal. Can be user-defined or determined automatically.
$\mathbf{x}_\ell[n]$	Vector containing all the previous $M_{\ell q}$ samples of $x_\ell[n]$: $\mathbf{x}_\ell[n] = [x_\ell[n-1],\ \ldots,\ x_\ell[n-M_{\ell q}]]^\top$.
$\alpha_{\ell q}[n]$	Coefficients of the linear predictor from the ℓ-th to the q-th signal.
$\boldsymbol{\alpha}_{\ell q}$	Vector containing all the coefficients of the linear predictor from the ℓ-th to the q-th signal: $\boldsymbol{\alpha}_{\ell q} = [\alpha_{\ell q}[1],\ \ldots,\ \alpha_{\ell q}[M_{\ell q}]]^\top$.
$G_{\ell \to q}$	Pairwise G-causality strength from the ℓ-th signal to the q-th signal.
$\mathbf{G}$	Pairwise G-causality strength matrix s.t. $\mathbf{G}_{\ell,q} = G_{\ell \to q}$ for $1 \leq \ell, q \leq Q$.
$C_{\ell q}$	Pairwise G-causality connectivity from the ℓ-th signal to the q-th signal, $C_{\ell q} = \chi_p(G_{\ell \to q})$.
$\mathbf{C}$	Pairwise G-causality connection matrix s.t. $\mathbf{C}_{\ell,q} = [\![\chi(G_{\ell \to q}) \geq \gamma_p]\!]$, i.e., $\mathbf{C}_{\ell,q} = 1$ if $\chi(G_{\ell \to q}) \geq \gamma_p$ and $\mathbf{C}_{\ell,q} = 0$ otherwise.
γ_p	Threshold used to determine whether a causal link exists or not. It is a function of the user-defined p-value.
$G_{\ell \to q \mid \mathcal{I}}$	Conditional G-causality strength from the ℓ-th signal to the q-th signal given the set of nodes in $\mathcal{I}$.
$\mathbf{G}_{\mathcal{I}}$	Conditional G-causality strength matrix s.t. $\mathbf{G}_{\mathcal{I}}(\ell, q) = G_{\ell \to q \mid \mathcal{I}}$.
$C_{\ell \to q \mid \mathcal{I}}$	Conditional G-causality connectivity from the ℓ-th signal to the q-th signal given the set of nodes in $\mathcal{I}$.
$\mathbf{C}_{\mathcal{I}}$	Conditional G-causality connection matrix s.t. $\mathbf{C}_{\mathcal{I}}(\ell, q) = [\![\chi\left(G_{\ell \to q \mid \mathcal{I}}\right) \geq \gamma_p]\!]$.
$\mathcal{C}_q = \text{cand}\{i_q\}$	Set of candidate sons of the q-th node ($1 \leq q \leq Q$).
$\mathcal{S}_q = \text{son}\{i_q\}$	Set of sons of the q-th node ($1 \leq q \leq Q$).
$\mathcal{P}_q = \text{pa}\{i_q\}$	Set of parents of the q-th node ($1 \leq q \leq Q$).

B. Conditional Causality

Unfortunately, pairwise GC is unable to discriminate between *direct causation* (e.g., $x_1[n] \to x_3[n]$) and *indirect causation* (e.g., $x_1[n] \to x_2[n] \to x_3[n]$). In both cases, the pairwise G-causality approach would lead to $\mathbf{C}_{1,3} = 1$, implying that $x_1[n]$ has caused $x_3[n]$. However, when building the *causality network* we are only interested in direct causes, since all the spurious links created by indirect causes may obscure the flow of information among signals. In order to avoid these undesired links returned by pairwise causality, *conditional G-causality* was introduced in [30]. In short, conditional GC attempts to determine whether $x_\ell[n]$ has caused $x_q[n]$ given another set of intermediate signals.

In order to provide a precise mathematical definition of conditional GC, let us define the set containing the indexes of the conditioning variables as $\mathcal{I}$. Following a similar procedure as before, we define the *conditional self-predictor*

$$\hat{x}_{q|\mathcal{I}}[n] = \boldsymbol{\alpha}_{qq}^\top \mathbf{x}_q[n] + \sum_{r \in \mathcal{I}} \boldsymbol{\alpha}_{rq}^\top \mathbf{x}_r[n], \tag{7}$$

where $\boldsymbol{\alpha}_{rq} = [\alpha_{rq}[1],\ \ldots,\ \alpha_{rq}[M]]^\top$ and $\mathbf{x}_r[n] = [x_r[n-1],\ \ldots,\ x_r[n-M]]^\top$ for all $r \in \mathcal{I}$, and the *conditional cross-predictor* from the ℓ-th signal (with $\ell \notin \mathcal{I}$) to the q-th output

$$\begin{aligned}\hat{x}_{\ell \to q|\mathcal{I}}[n] =& \boldsymbol{\alpha}_{qq}^\top \mathbf{x}_q[n] + \sum_{r \in \mathcal{I}} \boldsymbol{\alpha}_{rq}^\top \mathbf{x}_r[n] + \boldsymbol{\alpha}_{\ell q}^\top \mathbf{x}_\ell[n] \\ =& \hat{x}_{q|\mathcal{I}}[n] + \boldsymbol{\alpha}_{\ell q}^\top \mathbf{x}_\ell[n].\end{aligned} \tag{8}$$

Now, by defining the residual errors from the conditional predictors as $\varepsilon_{q|\mathcal{I}}[n] = x_q[n] - \hat{x}_{q|\mathcal{I}}[n]$ and $\varepsilon_{\ell \to q|\mathcal{I}}[n] = x_q[n] - \hat{x}_{\ell \to q|\mathcal{I}}[n]$, the conditional G-causality strength can be defined, in a similar way to (3), as

$$G_{\ell \to q|\mathcal{I}} = \ln \frac{\text{Var}(\varepsilon_{q|\mathcal{I}}[n])}{\text{Var}(\varepsilon_{\ell \to q|\mathcal{I}}[n])}. \tag{9}$$

Again, $0 \leq G_{\ell \to q|\mathcal{I}} < \infty$, with larger values of $G_{\ell \to q|\mathcal{I}}$ indicating a stronger evidence of causality from ℓ to q given the set of signals in $\mathcal{I}$; and we define two conditional connection/strength GC matrices, $\mathbf{G}_{\mathcal{I}}$ and $\mathbf{C}_{\mathcal{I}}$, whose (ℓ, q)-th elements are, respectively, $\mathbf{G}_{\ell,q|\mathcal{I}} = G_{\ell \to q|\mathcal{I}}$ and $\mathbf{C}_{\ell,q|\mathcal{I}} = [\![\chi(G_{\ell \to q|\mathcal{I}}) \leq \gamma_p]\!]$.

Note that the pairwise GC connection/strength matrices are unique, whereas many conditional GC connection/strength matrices can be constructed. The most usual situation is setting $\mathcal{I} = \mathcal{S}_{\neg\ell} = \{1,\ \ldots,\ \ell-1,\ \ell+1,\ \ldots,\ Q\} = \{1,\ \ldots,\ Q\} \setminus \{\ell\}$ and constructing the *full conditional* GC connection/strength matrices as $\mathbf{G}_{\ell,q|\mathcal{S}_{\neg\ell}} = G_{\ell \to q|\mathcal{S}_{\neg\ell}}$ and $\mathbf{C}_{\ell,q|\mathcal{S}_{\neg\ell}} = [\![\chi(G_{\ell \to q|\mathcal{S}_{\neg\ell}}) \leq \gamma_p]\!]$, respectively. However, conditional causality can also be used to build hierarchical models by conditioning on specific sets of nodes in a structured way, as described in Section 3.

3. HIERARCHICAL GRANGER CAUSALITY FOR INTRACAVITARY ELECTROGRAMS

On the one hand, pairwise GC may provide misleading results, as discussed in Section 2.1. On the other hand, the "brute-force approach" to conditional causality (i.e., applying conditional causality on the whole data set all at once) may obscure some of the existing relationships. Let us consider again the three-node causal network $x_1[n] \to x_2[n] \to x_3[n]$. Now, by applying the full-conditional GC approach we would typically obtain a single dependence relation: $G_{1 \to 2|3} = 1$. The other desired link, $x_2 \to x_3$, would typically not be included, since $G_{2 \to 3|1} = 0$ unless a very short lag (M) is used to ensure that only signals from neighbor nodes are taken into account (i.e., that the contribution of $x_1[n-1], \ldots, x_1[n-M]$ to the prediction of $x_3[n]$ is negligible).

In this paper we propose two hierarchical methods that are able to exploit the advantages of both approaches while minimizing their drawbacks. Both algorithms start by searching for the node with the "strongest" G-causality links with the remaining nodes and selecting it as the root node.[4] Then, the

[4]Note that the proposed framework essentially tries to identify the propagation direction of the AP. In order to do so, we propose a hierarchical approach based on Granger causality (although other causality measures could also be used) to measure the direction of the transfer of information throughout the available electrodes. In this setting, the root node becomes the entry point of the waveform to the set of electrodes, and thus it is essential to determine the desired propagation direction.

children of the root node are processed, adding new causality links if the corresponding causality test is passed. This process is repeated iteratively until there are no more nodes to process and a *poly-tree* has been constructed. The assumed premises are the following:

1) No feedback links can exist from lower nodes to higher nodes in the hierarchy. This restriction is a consequence of the *refractory period* of the AP: a period of time following the excited phase when additional stimuli evoke no substantial response [33].[5]
2) Causal interactions typically occur between neighbor nodes. This behavior is due to the continuous propagation of the waveform through the cardiac tissue.

In the sequel, we first describe the common initial step (i.e., the selection of the root node) and then we detail the two hierarchical causality algorithms proposed: GS-CaRe and LS-CaRe.

A. Initialization: Selecting the Root Node

The initialization stage, which is common for both the GS-CaRe and the LS-CaRe algorithms, seeks to find the optimal root node for the causal graph. This is done by computing the pairwise GC among all nodes and selecting the one with the "strongest" causal connections to other nodes. More precisely, the steps performed to select the root node are the following:

1) Compute $G_{q\to\ell}$ and $G_{\ell\to q}$ (for $\ell, q = 1, \ldots, Q-1$), and set the corresponding entries in $\mathbf{G}$ and $\mathbf{C}$.
2) Calculate the GC strength of the q-th node ($q = 1, \ldots, Q-1$) as the sum of the strength of its causal links to the remaining nodes:

$$g_q = \sum_{\ell=1}^{Q} \mathbf{G}_{q,\ell} = \sum_{\ell=1}^{Q} G_{q\to\ell}. \tag{10}$$

Calculate also the number of links for each node as

$$K_q = \sum_{\ell=1}^{Q} \mathbf{C}_{q,\ell} = \sum_{\ell=1}^{Q} [\![\chi(G_{q\to\ell}) \leq \gamma_p]\!]. \tag{11}$$

3) Determine the node with the largest number of outgoing causal links (i.e., links from that source node to some other sink node), selecting it as the root node:[6]

$$i_1 = \underset{1\leq q\leq Q}{\arg\max}\ K_q, \tag{12}$$

with g_q being used only to discriminate among nodes with identical values of K_q.

[5]Note that this assumption holds regardless of the type of catheter used, as long as the measurements taken by this catheter are all concentrated in a certain area of the atria (i.e., it may not hold for basket catheters that try to cover all of the atria). The only exception for the circular catheter used in the experiments (see Section 4) concerns the initial and final points in the hierarchy when we have circular dependencies like the ones shown in Figs. 3(p), (n) and (o). In this case our algorithm is unable to discover this last connection, and thus would always have at least one missing link.

[6]In [26], the root node was obtained by maximizing g_q instead of K_q, but we have observed that this can lead to an erroneous selection of the root node when a single very strong causal connection (i.e., a single very large value of $\mathbf{G}$) dominates over the rest.

B. Global Search Hierarchical Algorithm (GS-CaRe)

The GS-CaRe algorithm was initially proposed in [26] and later on refined in [27]. Figure 1 shows the flow diagram of the GS-CaRe algorithm. After the selection of the root node, as described in Section 3.1, GS-CaRe sets the root node as the current node and processes this current node (e.g., node i) recursively as shown in Figure 1:

- Finds the candidate children of the current node, $\mathcal{C}_i = \text{cand}\{i\} = \{\ell : \mathbf{C}_{i,\ell} = 1\}$, using pairwise GC.[7]
- Sorts the candidate children according to their pairwise GC strength, in such a way that $G_{i\to\mathcal{C}_i(1)} \geq G_{i\to\mathcal{C}_i(2)} \geq G_{i\to\mathcal{C}_i(3)} \geq \cdots$
- Finds the true children sequentially using conditional GC, starting with the "strongest" candidate and conditioning on all the previously accepted true children.

If the current node has some true children, the strongest one is selected as the current node, removed from the true children list and the aforementioned process is repeated again. It the current node does not have any true children (either because they have already been processed or because the end of the causality chain has been reached), then the parent of the current node is set as the current node and the process is repeated again. The algorithm ends when the current node is again the root node and does not have true children to process anymore. At the end of this process, GS-CaRe returns the strength/connection GC matrices, $\mathbf{G}$ and $\mathbf{C}$, which define a poly-tree with its children and parents.

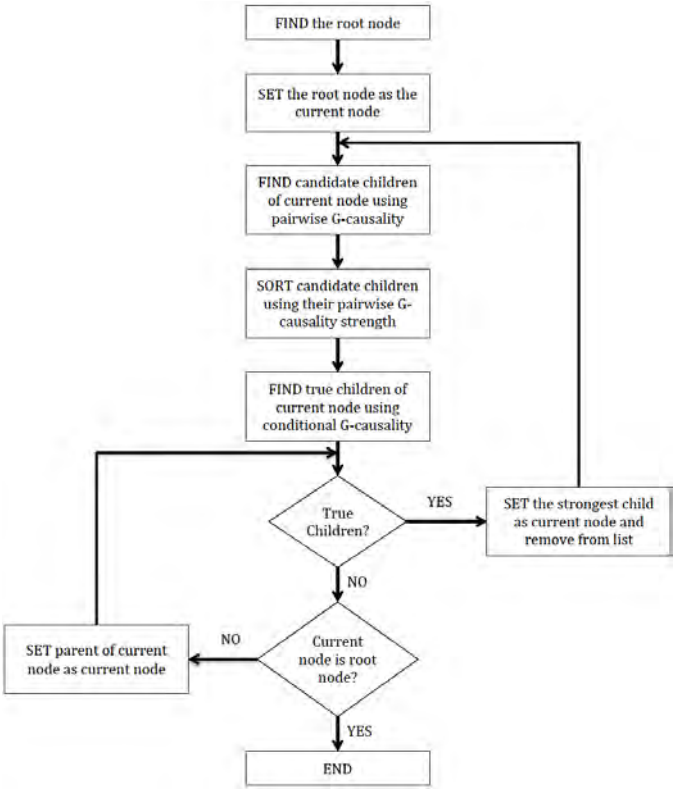

Fig. 1. Flow diagram of the GS-CaRe algorithm.

[7]Note that the search for candidate children is only performed on the currently unprocessed nodes. See [26] or [27] for further details.

C. Local Search Hierarchical Algorithm (LS-CaRe)

Figure 2 shows the flow diagram of the LS-CaRe algorithm. LS-CaRe processes the nodes directly according to their causal strength (starting from the root node, which is the "strongest" one), considering only causal links among neighbors up to a maximum user-defined distance, $d_{\max}$. First of all, let us define the distance among nodes as

$$d(\ell, q) = \min\{((\ell - q))_Q, ((q - \ell))_Q\}, \tag{13}$$

for any $\ell, q \in \{1, 2, \ldots, Q\}$ and with $((\cdot))_Q$ denoting the modulo operation, i.e., for any three integer numbers m, k and Q, $m = ((k))_Q \Leftrightarrow k = rQ + m$, where r and m are the only integers such that $-\infty < r < \infty$ and $0 \leq m \leq Q - 1$. Then, using the K_q computed in Section 3.1, construct an ordered set of nodes, $\mathcal{I} = \{i_1, i_2, \ldots, i_Q\}$ with i_1 being the root node, such that $K_\ell \geq K_q$ for all $\ell < q$.[8] Initialize the set of neighbors of each node by including only the own nodes (i.e., $\mathcal{N}_q^{(0)} = \{q\}$ for $q = 1, \ldots, Q$). Set $q = 1$ and $d = 1$. Now, the LS-CaRe algorithm proceeds in the following way:

1) Update the set of neighbors by including those neighbors at distance d from i_q, i.e., set $\mathcal{N}_q^{(d)} = \mathcal{N}_q^{(d)} \cup \mathcal{L}_q^{(d)}$ with
$$\mathcal{L}_q^{(d)} = \{\ell : d(i_q, \ell) = d,\ \ell = 1, \ldots, Q\}. \tag{14}$$
Hence, $\mathcal{N}_q^{(d)}$ includes now all those nodes whose distance to node i_q is lower or equal than d.
2) For any node $\ell \in \mathcal{L}_q^{(d)}$, add an edge from i_q to ℓ if $C_{i_q \to \ell} = 1$ and the following two conditions are fulfilled:
   a) There is no connection from any of the neighbors in $\mathcal{N}_q^{(d-1)}$ to/from i_q. Mathematically, defining
   $$\mathcal{E}_q^{(d)} = \sum_{\ell \in \mathcal{N}_q^{(d-1)}} \left(C_{\ell \to i_q} + C_{i_q \to \ell}\right), \tag{15}$$
   an edge can only be added if $\mathcal{E}_q^{(d)} = 0$. This condition implies that edges should not be added to nodes far away if connections to closer nodes already exist.
   b) The ℓ-th node is not already connected, i.e., $\sum_{j=1}^{Q} C_{j \to \ell} = 0$ or $\sum_{j=1}^{Q} C_{\ell \to j} = 0$.
3) If $q < Q$, then set $q = q + 1$ and return to step 1. Otherwise, set $q = 1$ and check d. If $d < d_{\max}$, set $d = d + 1$ and return to step 1.

At the end of this process, GS-CaRe returns again the strength/connection GC matrices, $\mathbf{G}$ and $\mathbf{C}$, for the whole set of nodes.

4. Numerical Experiments

In this section, we first define the performance measures that will be used in Section 4.1. Then, we describe the numerical experiments performed using synthetic data in Sections 4.2 and 4.3. Finally, the validation using annotated real data is provided in Section 4.4. In order to implement the four algorithms tested in this section (GS-CaRe, LS-CaRe, the pairwise approach and the full-conditional method), we have used the Granger causal connectivity (GCCA) toolbox [34].

[8] As indicated in Section 3.1, when $K_\ell = K_q$ for two nodes ℓ and q, we use g_ℓ and g_q to break the tie.

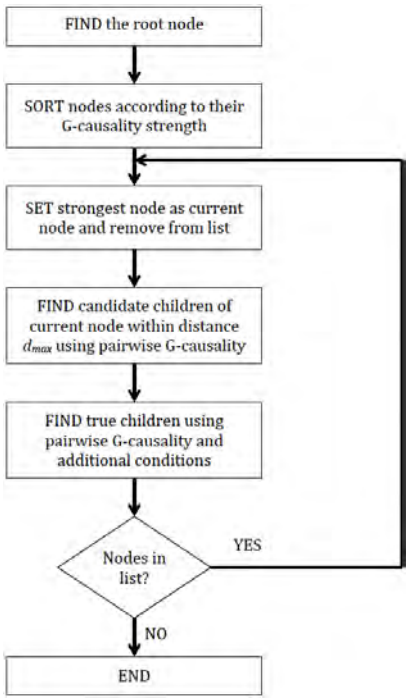

Fig. 2. Flow diagram of the LS-CaRe algorithm.

A. Methods and Performance Measures

In order to gauge the performance of the two novel hierarchical algorithms (LS-CaRe and GS-CaRe), we compare them against the following methods:

- **Pair:** pairwise causality discovery approach, which simply performs a pairwise causality check among all nodes.
- **Full:** full-conditional causality discovery technique, which performs a causality check among pairs of nodes conditioned on all the other nodes.
- **Alcaine et al.:** the approach proposed in [25], which defines a local propagation direction measure based on conditional causality relations among four adjacent nodes.

For this comparison we use several standard statistical performance measures. Let us denote the true causal connection from the ℓ-th to the q-th EGM (with $\ell \neq q$) as $\mathbf{C}_{\ell,q}$,[9] and the estimated one as $\widehat{\mathbf{C}}_{\ell,q}$. Noting that our main goal is discovering the causal links among the different EGMs, we can have the following situations:

- **True positive (TP):** The correct detection of an existing causal link, i.e., $\mathbf{C}_{\ell,q} = \widehat{\mathbf{C}}_{\ell,q} = 1$.
- **False negative (FN):** The failure to detect an existing causal link, i.e., $\mathbf{C}_{\ell,q} = 1$ and $\widehat{\mathbf{C}}_{\ell,q} = 0$.
- **True negative (TN):** The correct absence of a non-existing causal link, i.e., $\mathbf{C}_{\ell,q} = \widehat{\mathbf{C}}_{\ell,q} = 0$.
- **False positive (FP):** The detection of a causal link when no causal link truly exists, i.e., $\mathbf{C}_{\ell,q} = 0$ and $\widehat{\mathbf{C}}_{\ell,q} = 1$.

Let us denote the total number of positive cases (i.e., *true* causal links) as P, the total number of negative cases (i.e., non-existing or *false* causal links) as F, and the total number

[9] Remember that $\mathbf{C}_{\ell,q} = 1$ corresponds to the presence of a causal link and $\mathbf{C}_{\ell,q} = 0$ corresponds to the absence of that causal link.

of possible connections as $T = Q(Q-1)$. Now, we can define the following performance measures:[10]

- **Sensitivity:** Also known as True Positive Rate (TPR). Measures the proportion of causal links that are correctly identified out of the total number of causal links:

$$\text{TPR} = \frac{\text{TP}}{\text{P}} = \frac{\text{TP}}{\text{TP} + \text{FN}}. \tag{16}$$

- **Specificity:** Also known as True Negative Rate (TNR). Measures the proportion of non-existing causal links that are correctly identified:

$$\text{TNR} = \frac{\text{TN}}{\text{F}} = \frac{\text{TN}}{\text{TN} + \text{FP}}. \tag{17}$$

- **Accuracy:** Measures the proportion of true causal detections (both for existing and non-existing links) among the total number of possible connections:

$$\text{Acc} = \frac{\text{TP} + \text{TN}}{\text{T}} = \frac{\text{TP} + \text{TN}}{\text{TP} + \text{FP} + \text{TN} + \text{FN}}. \tag{18}$$

- **F-Score:** Also known as F_1 score. An alternative global measure of performance, obtained as the harmonic mean of sensitivity and precision (a. k. a. Positive Predictive Value (PPV), and defined as $\text{PPV} = \text{TP}/(\text{TP} + \text{FP})$):

$$F_1 = \frac{\text{PPV} \times \text{TPR}}{\text{PPV} + \text{TPR}} = \frac{2\text{TP}}{2\text{TP} + \text{FP} + \text{FN}}. \tag{19}$$

Altogether, these complementary measures provide a complete characterization of the performance of the different algorithms. On the one hand, a high sensitivity implies a low rate of false negatives, indicating that the method is unlikely to miss existing causal links (i.e., all the true causal relations in the data are likely to be discovered). On the other hand, a high specificity is related to a low level of false positives, meaning that the algorithm is unlikely to introduce spurious causal links (i.e., all the causal links introduced are likely to correspond to true links). Finally, the accuracy and the F-Score provide a single global performance measure that takes into account both the false positives and the false negatives.

B. Simple Synthetic Intracardiac Electrograms

In this section, we test the performance of the two algorithms proposed (LS-CaRe and GS-CaRe) on simple synthetic EGMs. In order to generate these signals, the network of modified stochastic FitzHugh-Nagumo (FH-N) oscillators described in [35] has been used as *in silico* model. FH-N oscillator networks are a simple, well-known and widely used model for waveform propagation in excitable media [33]. In cardiology, the FH-N equations can be used to replicate the AP of the sinoatrial node, and the FH-N dynamics has also been applied in the study of cellular coupling or the mechanism of defibrillation [36]. Regarding the analysis of AF, this model does not generate realistic EGMs in the time domain, but it is able to reproduce the propagation patterns observed in real patients (see the description below, Figure 3, and the videos attached as accompanying material). Therefore, we believe that it is a useful model to perform an initial validation of the proposed methods.

In our simulations, we construct a 2D grid composed of $J \times J$ nodes ($J = 32$), where each node corresponds to a dynamical system following the classic FH-N equations, discretized using Euler's method with an integration time step $T_d = 5 \times 10^{-3}$ s, plus an additive stochastic noise term, and a coupling term gathering the interaction with neighbor nodes. Altogether, this yields the following system of difference equations:

$$U_{i,j}[n+1] = U_{i,j}[n] + \sigma^2 \sqrt{T_d} B_{i,j}[n+1] + T_d \Bigg(p_3(U_{i,j}[n]) - V_{i,j}[n] + \frac{1}{D} \sum_{(\ell,r)\in\mathcal{N}_{i,j}} U_{\ell,r}[n] + m_{i,j} G[n+1] \Bigg), \tag{20a}$$

$$V_{i,j}[n+1] = V_{i,j}[n] + T_d \left(\beta_0 U_{i,j}[n] + \beta_1 V_{i,j}[n] + \beta_2 \right), \tag{20b}$$

where

- $n = 0, 1, 2, ...$ are the discrete-time instants, corresponding to continuous-time instants $t = nT_d$;
- $\{U_{i,j}[n]\}_{n=0,1,...}$ is the signal sequence (representing the AP of a cell) at the (i,j)-th node for $1 \le i, j \le J$;
- $p_3(u) = \sum_{r=0}^{3} \alpha_r u^r$ is a polynomial of order 3 with known fixed coefficients α_r for $r \in \{0,1,2,3\}$;
- $\{V_{i,j}[n]\}_{n=0,1,...}$ is the recovery sequence at the same node, which depends on the known parameters β_r for $r \in \{0,1,2\}$;
- the set $\mathcal{N}_{i,j} \subset \{1,...,J\} \times \{1,...,J\}$ contains the neighbors, within the grid, of the (i,j)-th node;
- the coupling coefficient, $D > 0$, is known and fixed;
- $G[n]$ is a known, non-negative and typically periodic forcing signal;
- the $\{m_{i,j}\}_{1\le i,j\le J} \in \{0,1\}$ are (known and fixed) binary indicators that determine which nodes are excited by the forcing signal $F[n]$;
- and the $\{B_{i,j}[n]\}_{n=0,1,...}$ are i.i.d. Gaussian random variables with zero mean and unit variance.

Using this model, we have generated a database composed of 17 sets of synthetic multi-variate EGMs that mimic AP wavefront propagation patterns observed in real signals. The parameters used for the simulations were set empirically in order to reproduce waveform propagation patterns observed in real signals (see [35] for further details): $\alpha_0 = \alpha_2 = 0$, $\alpha_1 = -\frac{18}{5}$, $\alpha_3 = 1$, $\frac{1}{D} = 4.5 \times 10^{-3}$, $\beta_0 = 2.1$, $\beta_1 = -0.6$, $\beta_2 = 0.6$, and $\sigma^2 = \frac{1}{2}$. Regarding $F[n]$, it consists of a periodic sequence of pulses. Rotors are generated by applying a forcing signal at one node right after the wavefront has passed through it. Then, we select 10 nodes from the 2D grid according to a circular layout resembling the topology of a 10-pole spiral catheter. With the virtual recording devices placed at these locations, the 9 synthetic bipolar EGMs used in the simulations are obtained. Figure 3 shows the different propagation patterns (see also the accompanying videos in the supplementary material), grouped into three categories:

- **Single**, corresponding to the AP wavefront propagation pattern observed when a single-loop rotor is present.

[10]Note that the range for all the performance measures is from 0 to 1, with 1 indicating the best possible result and 0 indicating the worst one.

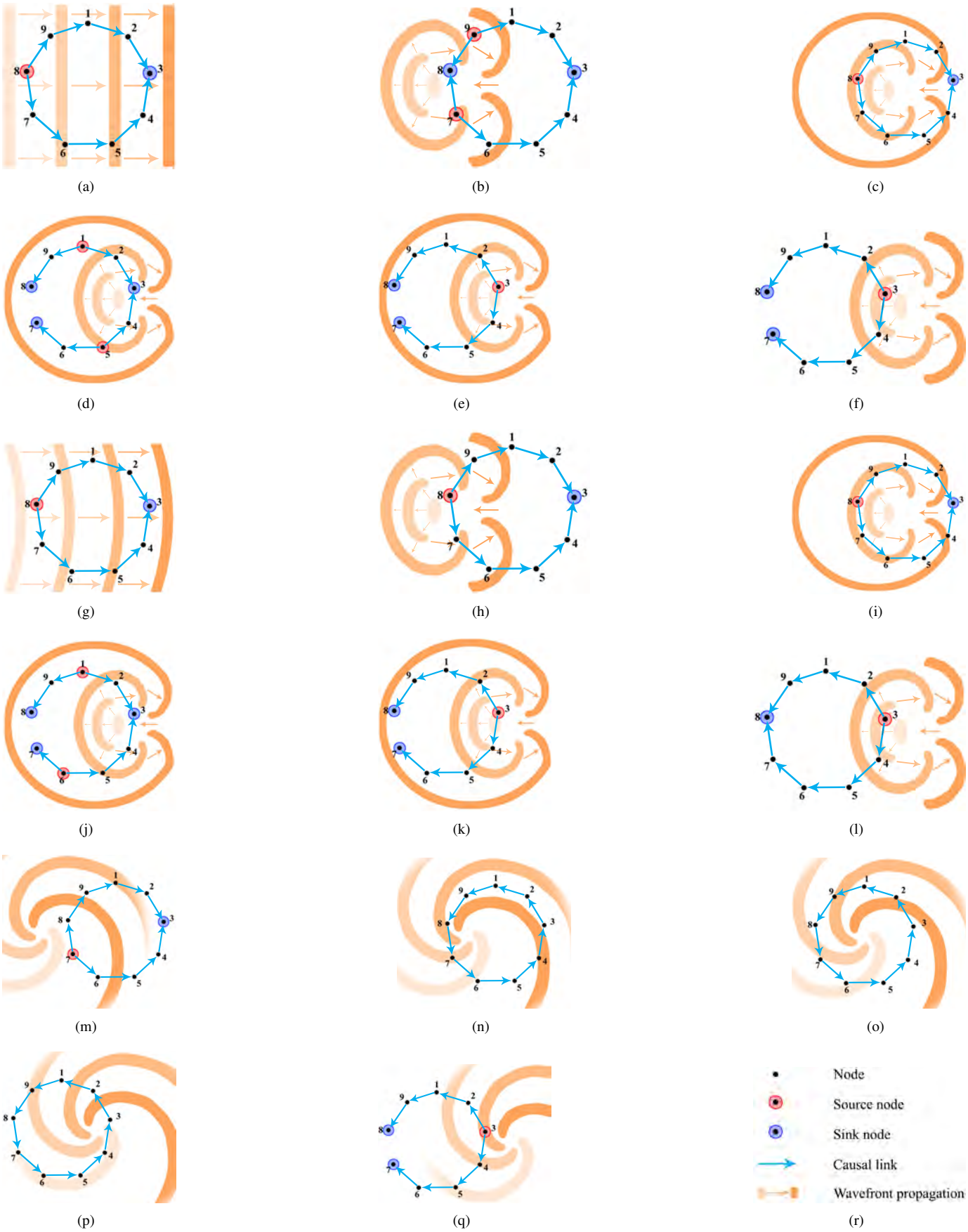

Fig. 3. Different propagation patterns generated by the synthetic signal simulator. **(a)–(f):** Flat 1–6. **(g)–(l):** Circular 1–6. **(m)–(q):** Single 1–5. **(r):** Legend.

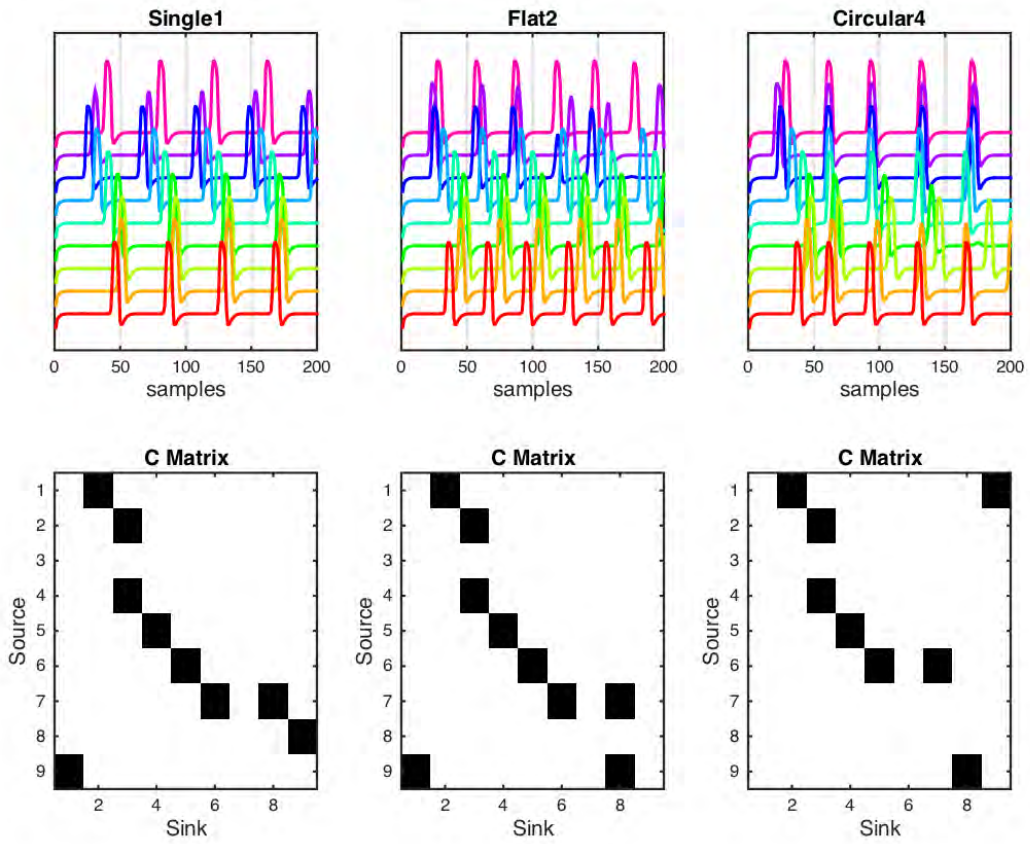

Fig. 4. **(Top)** Example of the nine synthetic signals (ordered from bottom to top as $1 \rightarrow 9$) generated for three different cases: Single 1, Flat 2, and Circular 4. **(Bottom)** Binary intensity plots of the true causality matrices $\mathbf{C}$. A black square corresponds to $\mathbf{C}_{\ell,q} = 1$, whereas a white square means $\mathbf{C}_{\ell,q} = 0$.

- **Flat**, associated to a flat propagation pattern (as observed when the catheter is placed far away from the focal source) plus a double-loop rotor (except in the first case).
- **Circular**, where a circular propagation pattern (corresponding to the catheter being placed close to the focal source) plus a double-loop rotor (once more, in all cases except for the first one) is observed.

The following information is shown in Figure 3:

- **Wavefront propagation:** Orange swirls of different intensities to show the local propagation pattern and direction of the electrical wavefront.
- **Nodes:** The locations of the nodes of the virtual recording device. Red and blue circles are used to denote source and sink nodes, respectively.
- The true causal links (blue lines and arrows) among the synthetic EGMs.

Figure 4 shows an example of the noiseless synthetic signals for three cases (single 1, flat 2 and circular 4), altogether with the intensity plots (using black squares for the ones and white squares for the zeros) of their true causality matrices.

In the first experiment, we analyze the performance of the different methods (in terms of the F-score) as a function of the two parameters of the model: the p-value and the lag (M). Tables II and III show the results. On the one hand, in Table II it can be seen that the results are rather stable w.r.t. the p-value, with slight decreases in performance for all the methods at low SNRs and small increases at large SNRs. On the other hand, from Table III we notice that a similar situation occurs (except for the full-conditional approach) for M. Therefore, instead of selecting specific values of p and M for the subsequent simulations, we present the results averaged over all the considered significance levels ($p \in \{0.05, 0.01, 0.001, 0.0001\}$) and orders of the AR models ($M \in \{10, 15, 20, 25, 30\}$).

Figures 5(a)–(c) show the averaged sensitivity (TPR), specificity (TNR) and F-score for the different methods tested. Alcaine's approach attains the best performance in terms of TPR and F-score (followed closely by LS-CaRe in both cases), whereas LS-CaRe attains the best TNR (with Alcaine's method performing slightly worse). The pairwise approach achieves good TPR values, but its performance is very poor in terms of TNR. On the contrary, the full-conditional and GS-CaRe techniques obtain good TNR values, but very poor TPRs. The F-score for these three cases (pairwise, full-conditional and GS-CaRe) is much lower than the F-score of Alcaine's method and LS-CaRe. Note the threshold effect in the sensitivity and F-score: below a certain SNR (around 0 dB) all methods fail. This effect is rather common in statistical inference problems (e.g., see Fig. 1 in [37], Fig. 2 in [38] or Fig. 6 in [39]), and here is due to the incorrect estimation of the underlying AR models used for GC computation: no causal links are detected at all, and thus the sensitivity and F-score are zero, whereas the specificity is close to one.

TABLE II
F-SCORE FOR THE DIFFERENT METHODS TESTED AS A FUNCTION OF THE p-VALUE USED FOR $M = 10$ AND TWO VALUES OF SNR.

Method	p**-value (SNR = 10 dB)**				p**-value (SNR = 40 dB)**			
	0.05	0.01	0.001	0.0001	0.05	0.01	0.001	0.0001
Full	0.3891	0.3768	0.3022	0.2373	0.4184	0.4551	0.4726	0.4691
Pair	0.4724	0.4908	0.4773	0.4522	0.4340	0.4620	0.4838	0.4791
GS-CaRe	0.3357	0.3391	0.3178	0.2866	0.3075	0.3328	0.3290	0.3584
LS-CaRe($d_{\max} = 1$)	0.8505	0.8237	0.7628	0.7004	0.7820	0.8272	0.8386	0.8111
LS-CaRe($d_{\max} = 2$)	0.8488	0.8268	0.7702	0.7137	0.7808	0.8301	0.8355	0.8152
LS-CaRe($d_{\max} = 3$)	**0.8525**	**0.8301**	**0.7842**	0.7334	0.7822	0.8287	0.8424	0.8268
Alcaine et al. [25]	0.7742	0.7829	0.7745	**0.7767**	**0.8756**	**0.8805**	**0.8801**	**0.8805**

TABLE III
F-SCORE FOR THE DIFFERENT METHODS TESTED AS A FUNCTION OF THE LAG (M) USED FOR $p = 0.05$ AND TWO VALUES OF SNR.

Method	M **(SNR = 10 dB)**					M **(SNR = 40 dB)**				
	10	15	20	25	30	10	15	20	25	30
Full	0.3891	0.2567	0.0634	0.0126	0.0029	0.4184	0.3935	0.1082	0.0206	0.0056
Pair	0.4724	0.3916	0.3308	0.3096	0.2973	0.4340	0.3915	0.3295	0.3036	0.2829
GS-CaRe	0.3357	0.2978	0.2689	0.2584	0.2264	0.3075	0.2958	0.2726	0.2443	0.2238
LS-CaRe($d_{\max} = 1$)	0.8505	0.8157	0.7755	0.7423	0.6879	0.7820	0.8615	0.8168	0.7750	0.7013
LS-CaRe($d_{\max} = 2$)	0.8488	**0.8221**	0.8041	0.7714	0.7116	0.7808	0.8649	0.8309	0.7957	0.7145
LS-CaRe($d_{\max} = 3$)	**0.8525**	0.8219	0.7943	0.7733	0.7161	0.7822	**0.8669**	0.8193	0.7870	0.7227
Alcaine et al. [25]	0.7742	0.8108	**0.8402**	**0.8852**	**0.8944**	**0.8756**	0.8534	**0.8916**	**0.8914**	**0.9089**

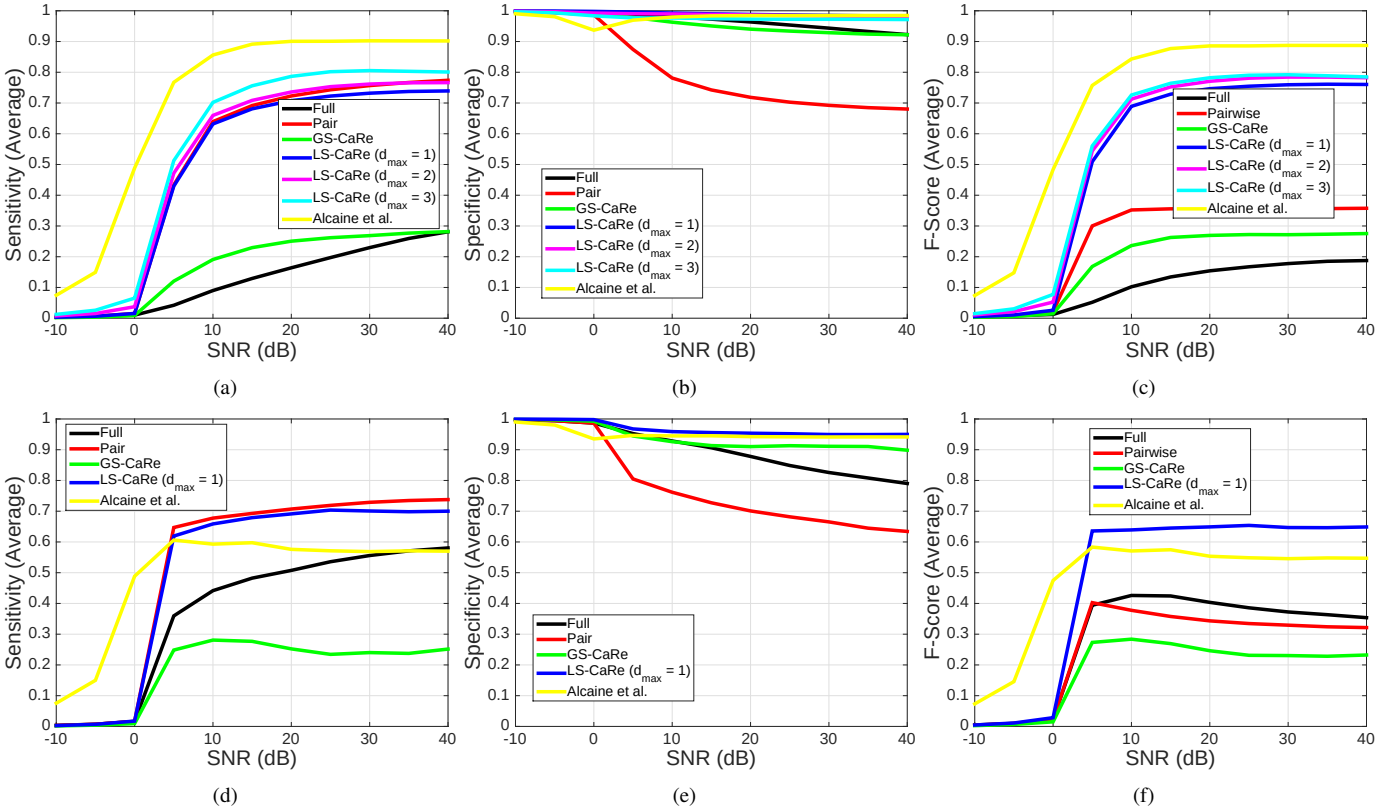

Fig. 5. Averaged results, over the considered significance levels ($p \in \{0.05, 0.01, 0.001, 0.0001\}$) and orders of the AR models ($M \in \{10, 15, 20, 25, 30\}$), for the synthetic signals using different performance measures (sensitivity, specificity and F-score). **(a)–(c)** Using the simple model of Section 4.2. **(d)–(f)** Using the more realistic model of Section 4.3.

Finally, Figure 6 shows examples of true causal connections and recovered causality maps (using SNR = 20 dB, $M = 10$, $p = 0.05$ and $d_{\max} = 1$ for LS-CaRe) for three cases: single 1, flat 2, and circular 4. All the methods add many spurious links, except for LS-CaRe and Alcaine's approach, which recover causality maps similar to the true ones.

C. Realistic Synthetic Electrograms

As a second case study, realistic electrograms were simulated using a complete 3D model of human atria [40]. Simulations were performed as in a previous study [41]: cellular electrophysiology was simulated using an AF-remodeled version of the Maleckar et al. model [42], whereas propagation of

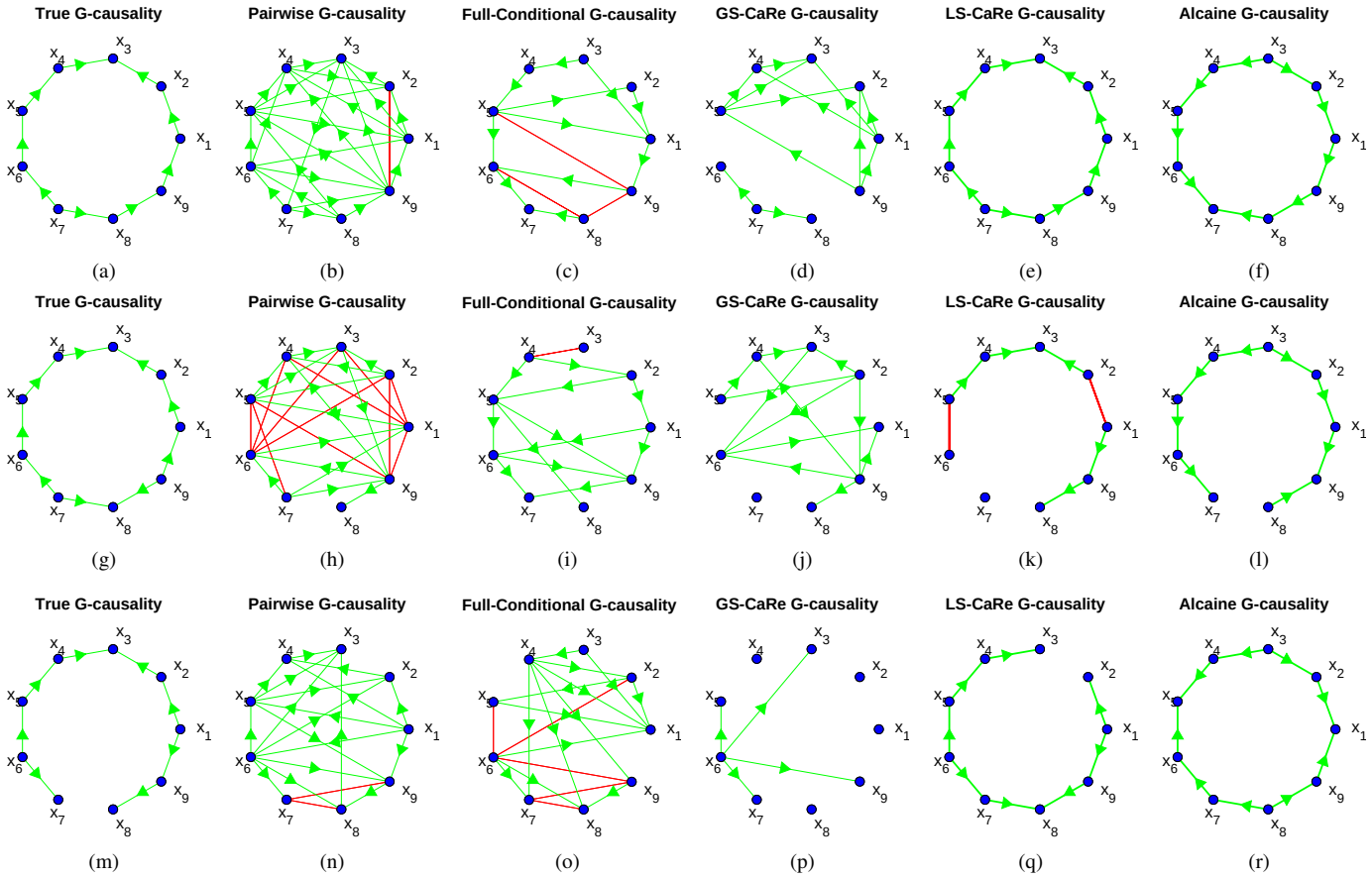

Fig. 6. Synthetic signals: example of the true causality graphs [(a), (g) & (m)] and the graphs recovered using the pairwise approach [(b), (h) & (n)], the full-conditional technique [(c), (i) & (o)], GS-CaRe [(d), (j) & (p)], LS-CaRe [(e), (k) & (q)], and Alcaine et al. [25] [(f), (l) & (r)] for three different cases. **(a)–(f)** Single 1. **(g)–(l)** Flat 2. **(m)–(r)** Circular 4. Red lines correspond to bidirectional causal links.

the action potential was computed by solving the monodomain equation with a finite element method-based software called ELVIRA [43]. The integration time-step used for the 3D atria simulations was 0.04 ms, so that the fast upstrokes of the action potentials could be properly generated, but the output voltages were only post-processed every 1 ms, facilitating comparison with real-world signals, typically acquired at 1 kHz (see Section 4.D). Three situations were simulated for 10 seconds each: sinus rhythm (periodic stimulation at the sinoatrial node every 500 ms), stable rotor at the right atrial appendage (not significant wavefront meandering during the whole simulation of AF), and chaotic activity at the right atrium (collisions of wavefronts, unstable rotors, and large wavefront meandering). In order to analyze the efficacy of the hierarchical algorithms, two grids of 16x16 virtual electrodes located at 2 mm distance from the atrial surface were used to compute unipolar electrograms: one in the right atrial appendage, and the other in the center of the right atrium.

Figure 5(d)–(f) shows that the results for this more realistic model are similar to those of the simpler one: LS-CaRe and Alcaine's method still attain good values of TPR, TNR and F-score (although lower than in the previous example); the pairwise approach achieves good values of TPR, but poor values of TNR and F-score; and GS-CaRe and the full-conditional scheme obtain a good TNR, but not so good values of TPR and F-score. Indeed, the main difference w.r.t. the simpler model is that LS-CaRe obtains a better performance than Alcaine's method for the three performance measures.

D. Real-World Signals

Intracavitary EGMs were recorded in 5 patients with persistent AF prior to an ablation procedure in the electrophysiology laboratory at HGUGM. Using a 10 pole spiral catheter (Lasso, Biosense Webster), 9 bipolar signals were obtained and bass-pand filtered within the 30-500 Hz band (LabSystem Pro, Boston Scientific). Data was digitized at 16-bit resolution with 1 kHz sampling frequency, and exported using custom software implemented in Labview (National Instruments). Signals were visually inspected and annotated for rotor presence by electrophysiologists from HGUGM. A total of 10 short EGM segments where the signal can be considered stationary were used as dataset for our algorithm, including 6 cases exhibiting normal AP wavefront propagation (wedge shaped) and 4 with circular propagation patterns (rotors). For all the cases, ground truth graphs displaying the electrode activation sequences from source to sink node(s) were constructed. An example of one true causality graph, altogether with the reconstructed causality graphs is shown in Figure 7. Note again the good performance of LS-CaRe and Alcaine's methods, especially compared to the large number of spurious links introduced by the pairwise, full-conditional and GS-CaRe approaches.

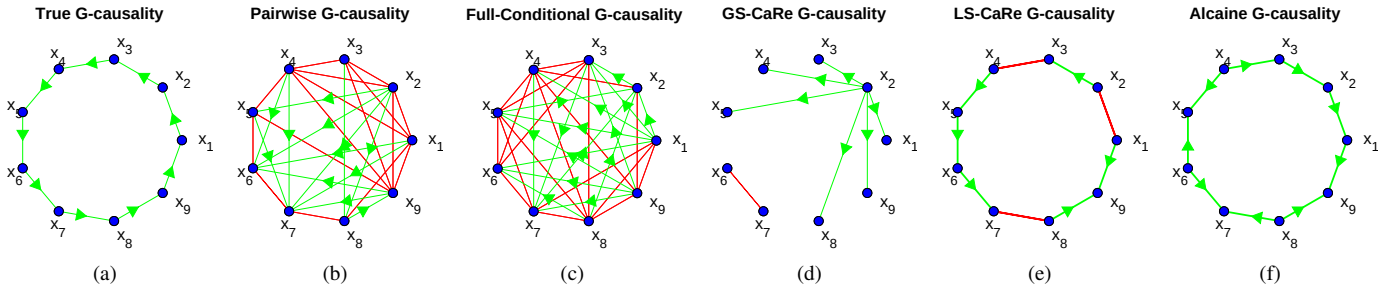

Fig. 7. Real-world signals: example of the true causality graph **(a)**, and the graphs recovered using the pairwise approach **(b)**, the full-conditional technique **(c)**, GS-CaRe **(d)**, LS-CaRe **(e)**, and Alcaine et al. [25] **(f)** for a real signal. Red lines correspond to bidirectional causal links.

TABLE IV
F-SCORE FOR THE DIFFERENT METHODS TESTED AVERAGED OVER THE FIVE LAGS AND THE FOUR SIGNIFICANCE LEVELS CONSIDERED.

Signal	Pairwise	Full	GS-CaRe	LS-CaRe	Alcaine et al. [25]
1	0.3234	0.2451	0.1734	0.5120	**0.7022**
2	0.4003	0.3902	0.2773	0.7030	**0.7072**
3	0.3440	0.2567	0.2474	0.3795	**0.4464**
4	0.3940	0.4097	0.3213	**0.8224**	0.8007
5	0.2575	0.1890	0.2124	0.3963	**0.5808**
6	0.4261	0.2909	0.4115	**0.6853**	0.5533
7	0.3226	0.2284	0.2602	**0.5648**	0.5000
8	0.2822	0.2033	0.1576	0.4983	**0.5006**
9	0.3470	0.2711	0.1395	**0.5249**	0.3486
10	0.4743	0.5153	0.3677	**0.7129**	0.7006
Avg. ± Std.	0.3571 ± 0.0665	0.3000 ± 0.1050	0.2568 ± 0.0903	0.5799 ± 0.1457	**0.5840 ± 0.1410**

TABLE V
AVERAGED RESULTS FOR SEVERAL PERFORMANCE METRICS, THE FIVE LAGS AND THE FOUR SIGNIFICANCE LEVELS CONSIDERED.

Signal	Pairwise	Full	GS-CaRe	LS-CaRe	Alcaine et al. [25]
Sensitivity	**0.6607 ± 0.2062**	0.4772 ± 0.1984	0.2439 ± 0.1026	0.6059 ± 0.1772	0.6110 ± 0.1333
Specificity	0.7723 ± 0.0854	0.8152 ± 0.0750	0.9350 ± 0.0205	**0.9508 ± 0.0162**	0.9470 ± 0.0188
Accuracy	0.7614 ± 0.0619	0.7819 ± 0.0597	0.8656 ± 0.0209	**0.9162 ± 0.0250**	0.9135 ± 0.0290
F-Score	0.3571 ± 0.0665	0.3000 ± 0.1050	0.2568 ± 0.0903	0.5799 ± 0.1457	**0.5840 ± 0.1410**

The results for the 10 real signals tested are displayed in Tables IV (F-Score for each case) and V (sensitivity, specificity, accuracy and F-Score averaged over the 10 cases). The following conclusions can be drawn from these two tables:

- The pairwise approach attains the highest sensitivity, with Alcaine's method and LS-CaRe obtaining slightly worse results. The full-conditional approach and GS-CaRe obtain much lower sensitivity values, due to the large number of true causal connections missed.
- In terms of specificity, LS-CaRe, GS-CaRe and Alcaine's methods behave much better than the other two (with LS-CaRe performing slightly better than Alcaine's). This is due to the fact that the other two approaches introduce many more false positives.
- In terms of global performance, LS-CaRe provides the best accuracy and Alcaine's method attains the highest F-score. The global performance of the other three methods is much worse, with the pairwise approach attaining the lowest accuracy and GS-CaRe the lowest F-score.

5. CONCLUSIONS

A generic hierarchical framework and two specific algorithms for causality retrieval in intracavitary EGMs, based on G-causality, have been described in this paper. Both algorithms rely on the initial discovery of the root node, but the influence of this node on their performance is very different: GS-CaRe depends critically on a proper selection of this root node, since a global search is then started from it and an erroneous choice invariably leads to poor results, whereas LS-CaRe only needs this root node as the starting point for its local search and thus is much more robust w.r.t. an erroneous selection. This robustness, altogether with the reduced number of false alarms introduced by the local search, explains the much better performance of LS-CaRe, which shows a comparable performance to the method proposed in [25] by Alcaine et al. Indeed, both LS-CaRe and Alcaine's approach have the same goal: restricting the search for causal connections to neighbors. However, the procedures followed to achieve this goal are very different: defining a novel local propagation direction measure (Alcaine's) and performing a structured hierarchical search (LS-CaRe). From a clinical point of view, the developed methods can be used by cardiologists for two purposes: (1) discriminating among different propagation patterns (e.g., flat or circular propagation vs. rotors); and (2) determining the direction of the received AP wavefront. In future work, we plan to incorporate other alternative measures of causality, like transfer entropy or the phase slope index, as well as Alcaine's novel local propagation direction measure, into the flexible framework described here.

ACKNOWLEDGEMENTS

The authors would like to thank Dr. Angel Arenal, from Hospital General Universitario Gregorio Marañón, for providing access to the real data, annotations and expert clinical advice on electrophysiology in general and AF in particular. This work has been partly funded by the BBVA Foundation through "I Convocatoria de Ayudas a Investigadores, Innovadores y Creadores Culturales" (MG-FIAR project), the Spanish "Ministerio de Industria, Economía y Competitividad" through the MIMOD-PLC (TEC2015-64835-C3-3-R) and ADVENTURE (TEC2015-69868-C2-1-R) projects, and Comunidad de Madrid through project CASI-CAM-CM (S2013/ICE-2845).

REFERENCES

[1] P. Kirchhof *et al.*, "2016 ESC Guidelines for the management of atrial fibrillation developed in collaboration with EACTS," *Europace*, vol. 18, no. 11, pp. 1609–1678, 2016. [Online]. Available: http://www.ncbi.nlm.nih.gov/pubmed/27567465

[2] W. B. Kannel and E. J. Benjamin, "Status of the epidemiology of atrial fibrillation," *Med. Clinics of N. America*, vol. 92, no. 1, pp. 17–40, 2008.

[3] L. Y. Chen *et al.*, "Atrial fibrillation and the risk of sudden cardiac death: The atherosclerosis risk in communities study and cardiovascular health study," *JAMA Internal Medicine*, vol. 173, no. 1, pp. 29–35, 2013.

[4] P. A. Wolf, R. D. Abbott, and W. B. Kannel, "Atrial fibrillation as an independent risk factor for stroke: The Framingham study," *Stroke*, vol. 22, pp. 983–988, 1991.

[5] S. Nattel, D. Li, and L. Yue, "Basic mechanisms of atrial fibrillation—very new insights into very old ideas," *Annual Review of Physiology*, vol. 62, no. 1, pp. 51–77, January 2000.

[6] D. E. Krummen and S. M. Narayan, "Mechanisms for the initiation of human atrial fibrillation," *Heart Rhythm*, vol. 6, no. 8, Supplement, pp. S12–S16, August 2009.

[7] G. Moe, "On the multiple wavelet hypothesis of atrial fibrillation," *Arch Int Phamacodyn Ther*, no. 140, pp. 183–188, 1962.

[8] M. A. Allessie *et al.*, "Experimental evaluation of Moe's wavelet hypothesis of atrial fibrillation," in *Cardiac Electrophysiology and Arrhythmias*, D. Zipes and J. Jalife, Eds. Grune & Stratton, 1985, pp. 265–275.

[9] J. Jalife, O. Berenfeld, and M. Mansour, "Mother rotors and fibrillatory conduction: a mechanism of atrial fibrillation," *Cardiovascular Research*, vol. 54, no. 2, pp. 204–216, 2002.

[10] H. Calkins *et al.*, "2012 HRS/EHRA/ECAS Expert Consensus Statement on Catheter and Surgical Ablation of Atrial Fibrillation: Recommendations for Patient Selection, Procedural Techniques, Patient Management and Follow-up, Definitions, Endpoints, and Research Trial Design," *Europace*, vol. 14, no. 4, 2012.

[11] K. Nademanee *et al.*, "A New Approach for Catheter Ablation of Atrial Fibrillation: Mapping of the Electrophysiologic Substrate," *Journal of the American College of Cardiology*, vol. 43, no. 11, pp. 2044–53, 2004. [Online]. Available: http://www.ncbi.nlm.nih.gov/pubmed/15172410

[12] J. Ng and J. J. Goldberger, "Understanding and Interpreting Dominant Frequency Analysis of AF Electrograms," *Journal of Cardiovascular Electrophysiology*, vol. 18, no. 6, pp. 680–685, 2007. [Online]. Available: http://doi.wiley.com/10.1111/j.1540-8167.2007.00832.x

[13] Y. Takahashi *et al.*, "Organization of frequency spectra of atrial fibrillation: relevance to radiofrequency catheter ablation," *Journal of Cardiovascular Electrophysiology*, vol. 17, no. 4, pp. 382–388, 2006.

[14] G. W. Botteron and J. M. Smith, "A technique for measurement of the extent of spatial organization of atrial activation during atrial fibrillation in the intact human heart," *IEEE Transactions on Biomedical Engineering*, vol. 42, no. 6, pp. 579–586, 1995.

[15] S. L. Bressler and A. K. Seth, "Wiener–Granger causality: a well established methodology," *NeuroImage*, vol. 58, no. 2, pp. 323–329, 2011.

[16] L. Faes, A. Porta, and G. Nollo, "Testing frequency-domain causality in multivariate time series," *IEEE Transactions on Biomedical Engineering*, vol. 57, no. 8, pp. 1897–1906, 2010.

[17] S. Kleinberg and G. Hripcsak, "A review of causal inference for biomedical informatics," *Journal of Biomedical Informatics*, vol. 44, no. 6, pp. 1102–1112, 2011.

[18] L. Faes and G. Nollo, "Assessing frequency domain causality in cardiovascular time series with instantaneous interactions," *Methods of Information in Medicine*, vol. 49, no. 5, p. 453, 2010.

[19] A. Porta *et al.*, "Granger causality in cardiovascular variability series: Comparison between model-based and model-free approaches," in *IEEE Engineering in Medicine and Biology Conf. (EMBC)*, 2012, pp. 3684–3687.

[20] U. Richter *et al.*, "A novel approach to propagation pattern analysis in intracardiac atrial fibrillation signals," *Annals of Biomedical Engineering*, vol. 39, no. 1, pp. 310–323, 2011.

[21] ——, "Propagation Pattern Analysis During Atrial Fibrillation Based on Sparse Modeling," *IEEE Transactions on Biomedical Engineering*, vol. 59, no. 5, pp. 1319–1328, May 2012.

[22] M. Rodrigo *et al.*, "Causality relation map: a novel methodology for the identification of hierarchical fibrillatory processes," in *Computing in Cardiology (CinC)*, Sep. 2011, pp. 173–176.

[23] ——, "Identification of fibrillatory sources by measuring causal relationships," in *2012 Computing in Cardiology*, Sep. 2012, pp. 705–708.

[24] ——, "Identification of dominant excitation patterns and sources of atrial fibrillation by causality analysis," *Annals of Biomedical Engineering*, vol. 44, no. 8, pp. 2364–2376, Aug. 2016.

[25] A. Alcaine *et al.*, "A multi-variate predictability framework to assess invasive cardiac activity and interactions during atrial fibrillation," *IEEE Transactions on Biomedical Engineering*, vol. 64, no. 5, pp. 1157–1168, May 2017.

[26] D. Luengo, G. Ríos-Muñoz, and V. Elvira, "Causality analysis of atrial fibrillation electrograms," in *Computing in Cardiology (CinC)*, 2015, pp. 585–588.

[27] D. Luengo *et al.*, "A hierarchical algorithm for causality discovery among atrial fibrillation electrograms," in *IEEE Int. Conf. on Acoustics, Speech and Signal Processing (ICASSP)*, 2016, pp. 774–778.

[28] C. W. J. Granger, "Investigating causal relations by econometric models and cross-spectral methods," *Econometrica*, vol. 37, pp. 424–438, 1969.

[29] P. Stoica and Y. Selen, "Model-order selection: a review of information criterion rules," *IEEE Signal Processing Magazine*, vol. 21, no. 4, pp. 36–47, 2004.

[30] J. Geweke, "Measures of conditional linear dependence and feedback between time series," *Journal of the American Statistical Association*, vol. 79, pp. 907–915, 1984.

[31] J. D. Gibbons and J. W. Pratt, "p-values: interpretation and methodology," *The American Statistician*, vol. 29, no. 1, pp. 20–25, 1975.

[32] M. E. Masson, "A tutorial on a practical Bayesian alternative to null-hypothesis significance testing," *Behavior Research Methods*, vol. 43, no. 3, pp. 679–690, 2011.

[33] J. Keener and J. Sneyd, *Mathematical physiology I: cellular physiology*. Springer Science & Business Media, 2010.

[34] A. K. Seth, "A MATLAB toolbox for Granger causal connectivity analysis," *Journal of Neuroscience Methods*, vol. 186, no. 2, pp. 262–273, 2010.

[35] D. Crisan, J. Miguez, and G. Rios, "A simple scheme for the parallelization of particle filters and its application to the tracking of complex stochastic systems," Tech. Rep., 2014. [Online]. Available: https://arxiv.org/abs/1407.8071

[36] J. Keener and J. Sneyd, *Mathematical physiology II: systems physiology*. Springer Science & Business Media, 2010.

[37] C. Pantaleón, D. Luengo, and I. Santamaría, "Optimal estimation of chaotic signals generated by piecewise-linear maps," *IEEE Signal Processing Letters*, vol. 7, no. 8, pp. 235–237, 2000.

[38] D. Luengo, I. Santamaría, and L. Vielva, "A general solution to blind inverse problems for sparse input signals," *Neurocomputing*, vol. 69, no. 1, pp. 198–215, 2005.

[39] V. Elvira *et al.*, "Improving population Monte Carlo: Alternative weighting and resampling schemes," *Signal Processing*, vol. 131, pp. 77–91, 2017.

[40] G. Seemann *et al.*, "Heterogeneous three-dimensional anatomical and electrophysiological model of human atria," *Philosophical Transactions of the Royal Society of London A: Mathematical, Physical and Engineering Sciences*, vol. 364, no. 1843, 2006.

[41] C. Sánchez *et al.*, "Atrial fibrillation dynamics and ionic block effects in six heterogeneous human 3D virtual atria with distinct repolarization dynamics," *Frontiers in Bioengineering and Biotechnology*, vol. 5, pp. 1–13, May 2017.

[42] M. M. Maleckar *et al.*, "K+ current changes account for the rate dependence of the action potential in the human atrial myocyte," *AJP: Heart and Circulatory Physiology*, vol. 297, no. 4, pp. H1398–H1410, 2009.

[43] E. A. Heidenreich *et al.*, "Adaptive macro finite elements for the numerical solution of monodomain equations in cardiac electrophysiology," *Annals of Biomedical Engineering*, vol. 38, no. 7, pp. 2331–2345, 2010.